Journal of Materials Chemistry

Cite this: J. Mater. Chem., 2012, 22, 13477

www.rsc.org/materials

COMMUNICATION

# A macroscopically oriented lyotropic chromonic liquid crystalline nanofiber mat embedding self-assembled Sunset-Yellow FCF nanocolumns†

Young-Jin Kim,‡[a] Dae-Yoon Kim,‡[a] Jong-Hoon Lee,[a] Changwoon Nah,[a] Joong Hee Lee,[a] Myong-Hoon Lee,[a] Hak Yong Kim,[b] Shiao-Wei Kuo,[c] Seunghan Shin*[d] and Kwang-Un Jeong*[a]

*Received 22nd February 2012, Accepted 11th May 2012*
**DOI: 10.1039/c2jm31092a**



**A macroscopically oriented anisotropic nanofiber mat embedding self-assembled Sunset-Yellow FCF nanocolumns was fabricated by the electrospinning technique. From the 2D WAXD and polarized FTIR results, it was realized that the nanocolumns were aligned parallel to the long axis of the nanofiber.**

Lyotropic liquid crystalline (LLC) phases formed especially in aqueous solutions have been observed in the range of materials known as dyes, drugs, surfactants, soaps and nucleic acids.[1–5] In contrast to thermotropic LC phases created by changing temperature, LLC is a broad but poorly studied class of soft matter. Among various LLC molecules, lyotropic chromonic LCs (LCLCs) consisting of a hydrophobic disk-like rigid core with two or more hydrophilic ionic groups at the periphery have recently attracted the attention of a lot of scientists and engineers due to the excellent one-dimensional (1D) electron transportation along the long axis of self-assembled nanocolumns (nanowires) as well as the selective light absorption parallel to the in-plane of the discotic core of LCLCs. Similar to the dimer formation in amphiphilic micelle systems, LCLCs tend to aggregate together even in dilute solutions due to the strong π–π interaction between aromatic cores. However, they do not show a distinct threshold concentration of phase transition from the isotropic phase to the ordered LC phases.[1,2] Upon varying the concentrations and types of the solvents, LCLCs assemble to form micelles, lamellar, hexagonal or crystal aggregates driven by physical interactions, such as hydrogen bonding, nanophase separations, π–π interactions, van der Waals interactions and ionic bonds.[5,6] In a polar solvent, LCLCs are assembled into nanocolumns by molecular stacking in face-to-face arrangements, resulting in the exposition of ionic groups to the polar solvent.[7] When the LCLC nanocolumn is long enough, a columnar nematic (N) phase can be formed. On increasing the concentration of the LCLC solution, the assembled nanocolumns can organize into highly ordered structures, such as hexagonal, rectangular and oblique LC phases including crystalline phases at higher concentrations.[8–10]

Since electrons can be rapidly transported along the long axis of LCLC nanocolumns as well as macroscopically oriented anisotropic LCLC sheets obtained by a simple coating, LCLCs can be applied in various practical applications, such as solar cells, LC displays and electro-optic devices. However, LCLC sheets fabricated by the coating of the LCLC–$H_2O$ solution contain many defects, such as macroscopic cracks generated during and after the coating processes. Additionally, the coated LCLC films are vulnerable to chemical attacks and to mechanical impacts. To solve these problems, a polymer can be introduced to stabilize the anisotropic LCLC films. However, macroscopic phase separations often occur between LCLC and polymer.[1] In order to overcome this limitation, we propose the confinement of LCLC nanocolumns in the electrospun nanofibers by the combination of molecular self-assembly of LCLC (a bottom-up method) and the electrospinning technique (a top-down method).[11] Furthermore, when the electrospun nanofibers embedding LCLC nanocolumns with long axes parallel to the fiber direction can be uniformly aligned in a large area, we can successfully fabricate a robust anisotropic LCLC mat.

In order to realize our proposal, we select Sunset-Yellow FCF (abbreviated as SSY, Sigma-Aldrich) as a LCLC molecule and poly(vinylpyrrolidone) (abbreviated as PVP, Sigma-Aldrich, $M_w$ = 1 300 000 g $mol^{-1}$) as a stabilizing polymeric material (Fig. 1b). To avoid the complicated interactions between PVP and SSY, $Na^+$ ions in SSY are substituted with $H^+$ ions by the proton exchange reaction using H-form Dowex G-26 (Dow Chemicals). The detailed ion-exchange process is described in the ESI (Fig. S1†). The proton exchanged Sunset-Yellow FCF is denoted as H-SSY (Fig. 1a).

To investigate the phase behaviours of H-SSY in an aqueous solution, a ternary phase diagram of PVP–H-SSY–$H_2O$ under ambient conditions is first constructed with respect to the concentration, as shown in Fig. 1c. Based on the cross-polarized optical microscopy (POM) observations, it is realized that H-SSY

[a]*Department of Polymer-Nano Science and Technology and Department of Flexible and Printable Electronics and Department of BIN Fusion Technology, Chonbuk National University, Jeonju, 561-756, Korea. E-mail: kujeong@chonbuk.ac.kr; Fax: +82 63 270 2341; Tel: +82 63 270 4633*
[b]*Department of Organic Materials and Fibre Engineering, Chonbuk National University, Jeonju, 561-756, Korea*
[c]*Department of Materials Science and Optoelectronic Engineering, National Sun Yat-Sen University, Kaohsiung 804, Taiwan*
[d]*Chonan R&D Centre, Korea Institute of Industrial Technology, Chonan, 330-825, Korea. E-mail: shshin@kitech.re.kr*

† Electronic supplementary information (ESI) available: Detailed descriptions of materials, equipments, and sample preparations as well as the fabricating procedure and the results of 2D WAXD, DSC and polarized FTIR. See DOI: 10.1039/c2jm31092a

‡ These authors contributed equally to this work.

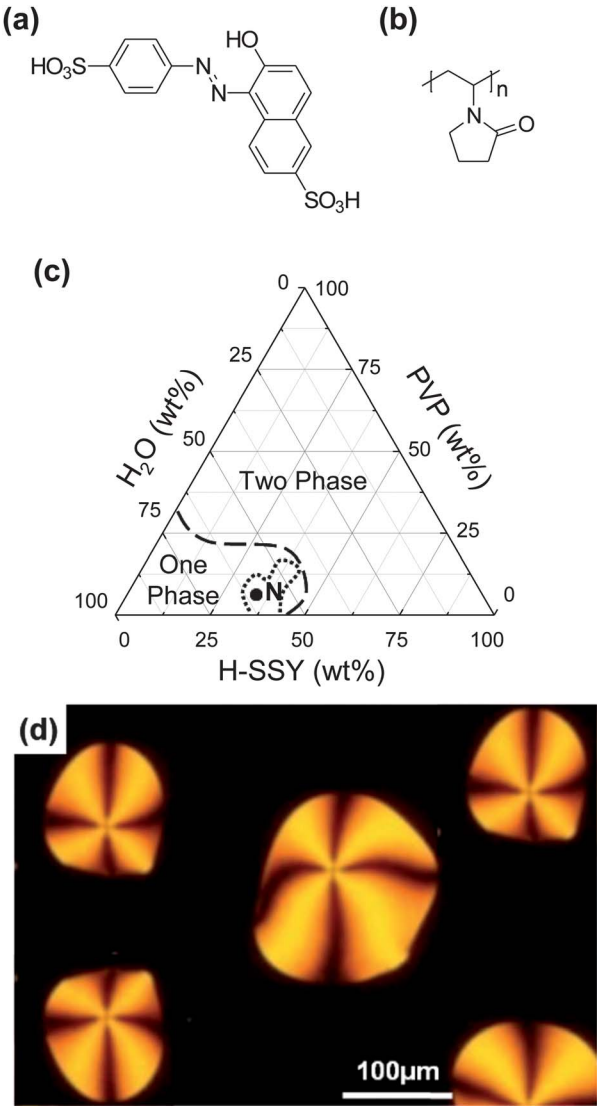


**Fig. 1** Chemical structures of (a) H-SSY and (b) PVP. (c) Ternary phase diagram for the H-SSY–PVP–$H_2O$ solution at room temperature. (d) POM image of the H-SSY–PVP–$H_2O$ solution which is represented as a black dot in (c).

precipitates and forms two phases when the H-SSY content in the PVP–H-SSY–$H_2O$ solution exceeds the dashed line. Especially, the compositions surrounded by a dotted line show a four-brush Schlieren texture (Fig. 1d), a typical texture of the columnar N LC phase. The compositions outside the dotted line but below the dashed line exhibit an isotropic (I) phase. It is worth noting that the compositions near the dotted line in Fig. 1c reveal the biphase of columnar N and I, which is one of the unique characteristics of LCLC molecules.

Based on the scanning electron microscopy (SEM) morphological observations of the electrospun PVP–H-SSY nanofibers (Fig. 2), the composition of the PVP–H-SSY–$H_2O$ solution and electrospinning conditions are optimized. The PVP–$H_2O$ (at 7/93 wt%) and the PVP–H-SSY–$H_2O$ (at 5/28/67 wt%) solutions, represented as a solid dot in Fig. 1c, give the best SEM morphologies without the formation of beads, as shown in Fig. 2a and b, respectively. The average diameters of the electrospun PVP and PVP–H-SSY nanofibers are

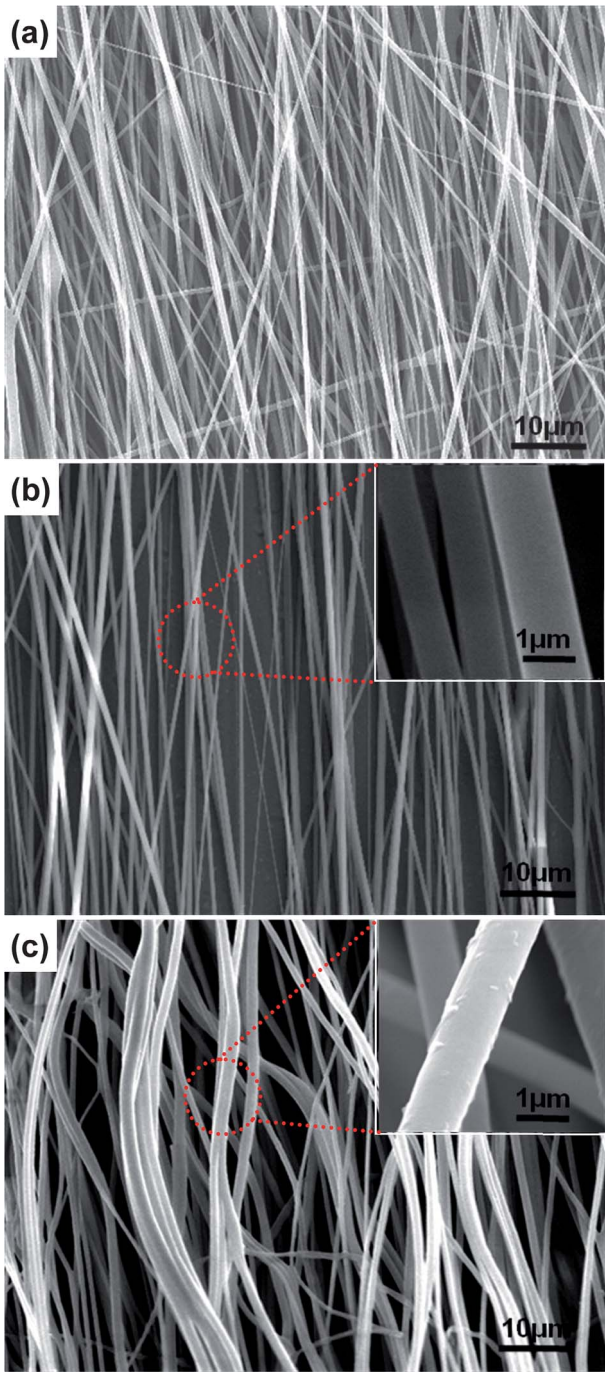


**Fig. 2** SEM images of the (a) PVP nanofiber, (b) PVP–H-SSY nanofiber at room temperature, and (c) annealed PVP–H-SSY nanofiber after annealing at 220 °C for 12 h. The insets of (b) and (c) are the magnified SEM images of (b) and (c), respectively.

estimated to be ~400 and ~900 nm, respectively. Note that the content of H-SSY in the PVP–H-SSY nanofiber is 15.2 wt% after the evaporation of $H_2O$. More detailed explanations of optimization processes are given in the ESI†. When the rotational speed of the collector is maintained faster than that of the electrospinning, the electrospun nanofibers can be aligned along the rotational direction of the collector, as shown in Fig. 2a and b. Considering the order parameter ($S$) of nanofibers,[12] the degrees of nanofiber orientation

 

are calculated to be 77% and 97% for the PVP and the PVP–H-SSY nanofiber sheets, respectively. This result is partially due to the fact that the assembled H-SSY nanocolumns in the nanofiber may behave like the metal cores of electric wires, which leads to a higher orientation of nanofibers. However, this consideration should be confirmed by structure sensitive experiments such as 2D wide angle X-ray diffraction (2D WAXD), which will be discussed later in this communication.

As shown in Fig. 2c, when the anisotropically oriented PVP–H-SSY nanofiber mat is annealed for 12 h at 220 °C, a temperature higher than the glass transition temperature ($T_g$ = 180 °C) of PVP, the oriented PVP–H-SSY nanofibers are bent due to the unbalanced surface stresses but still maintain the fibrous formations although the degree of nanofiber orientation decreases down to 40%. From the highly magnified SEM images of PVP–H-SSY nanofibers before (inset of Fig. 2b) and after (inset of Fig. 2c) the annealing processes, it is realized that the diameter of the nanofiber increases due to the transformation of the stretched PVPs to the relaxed coils and that the surface of the nanofiber is decorated with flat fragments in an average diameter of 50 nm. The flat fragments on the surface can be considered as H-SSY crystals which are migrated to the surface by the crystal-induced phase separation when the PVP–H-SSY nanofibers are annealed above the $T_g$ of PVP. This speculation based on the SEM images can be supported by differential scanning calorimetry (DSC) results of PVP and PVP–H-SSY nanofibers. Upon heating PVP–H-SSY nanofibers, an endothermic first-order thermal transition appears between 220 and 270 °C, which is not observed in the DSC thermogram of the annealed PVP–H-SSY nanofibers (Fig. S2†). At this point, a question can be raised: whether H-SSY in the PVP–H-SSY nanofiber is ordered or not?

In order to answer this question, a single PVP–H-SSY nanofiber is observed by POM, as represented in Fig. 3. If the fiber direction (FD) is arranged parallel to the polarizer or analyzer, there is no birefringence detected while birefringence is maximized when the FD is rotated 45° with respect to the polarizer and analyzer (Fig. 3 and its inset). Note that the pristine PVP nanofiber does not exhibit any detectable birefringence under POM. This means that PVP in the PVP–H-SSY nanofiber is in an amorphous state (Fig. S2†) and is not stretched enough to show birefringence. Therefore, based on POM observations, it can be concluded that H-SSY molecules in the PVP–H-SSY nanofiber are highly oriented with respect to FD. However, to know more details about molecular packing behaviours in the PVP–H-SSY nanofiber, a structure sensitive diffraction technique should be applied. Fig. 4a shows the 2D WAXD pattern of the PVP–H-SSY nanofiber mat which is obtained on an image plate by irradiating X-rays perpendicular to FD. On the meridian, a pair of diffused diffractions appears at $2\theta = 27.2°$ ($d$-spacing = 0.327 nm) which is a typical π–π interaction distance between H-SSY

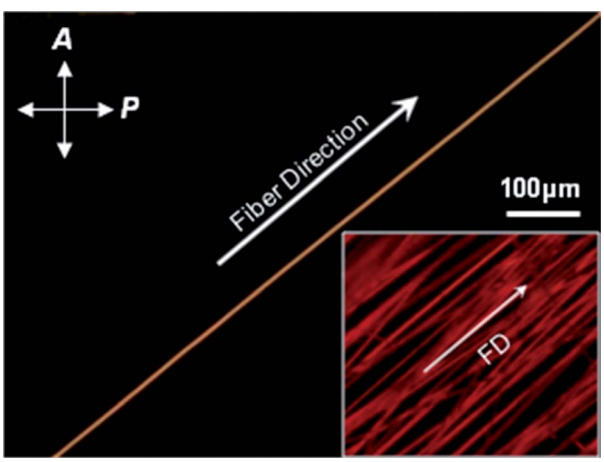


**Fig. 3** POM images of the PVP–H-SSY nanofiber when the long axis of the nanofiber is rotated 45° counterclockwise with respect to the polarizer. The inset is the POM image of a macroscopically oriented PVP–H-SSY nanofiber mat.

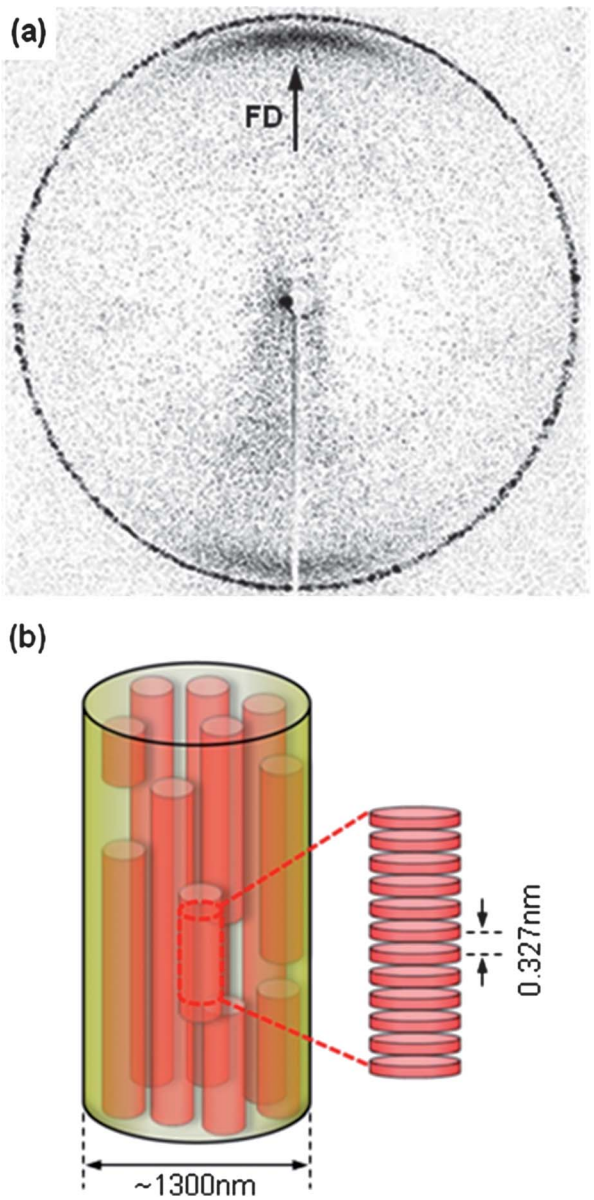


**Fig. 4** (a) 2D WAXD pattern of the PVP–H-SSY nanofiber, which is measured at room temperature. (b) Schematic illustration of molecular packing of H-SSY in the electrospun PVP–H-SSY nanofiber. Here, PVP is represented as a matrix and is not shown in detail and the diameter of the nanofiber is estimated by SEM.

molecules. From this result, it is clear that H-SSY molecules can self-assemble to nanocolumns even in PVP–H-SSY nanofibers and the long axis of nanocolumns is parallel to FD. The degree of nanocolumn orientation in PVP–H-SSY nanofibers is estimated to be 81% by azimuthal scanning of the $2\theta$ angle between $2\theta = 26°$ and 28° in 2D WAXD of the PVP–H-SSY nanofiber mat (Fig. S4†). The degree of nanocolumn orientation decreases down to 69% after the annealing process (Fig. S4†). Utilizing the Scherrer equation,[13] the correlation length along the H-SSY nanocolumns before and after the annealing process can be calculated to be 40 and 31 nm, respectively. On the equator of 2D WAXD (Fig. 4a), there is a pair of very broad diffractions with a low intensity between $2\theta = 4°$ and 7°. This result indicates that the correlation between nanocolumns in PVP–H-SSY nanofibers is very weak. This explanation is further confirmed by 2D WAXD of H-SSY crystalline powders and annealed PVP–H-SSY nanofibers (Fig. S3†). Note that the normal distance between H-SSY discs is a little bit expanded from 0.327 to 0.332 nm after the annealing process, which is in consequence of the self-organization of nanocolumns during the recrystallization of H-SSY. Based on the results of 2D WAXD combined with those of DSC and POM, the H-SSY molecular packing is proposed as schematically illustrated in Fig. 4b. The phase of PVP–H-SSY nanofibers is identified as a glassy columnar N phase which is in a thermodynamically metastable state compared with the H-SSY crystalline phase. The molecular arrangement illustrated in Fig. 4b is also confirmed by polarized Fourier transform infrared (FTIR) results (Fig. S4†) obtained by rotating the azimuthal axis from 0° to 90° with respect to the nanofiber direction. From the results of polarized FTIR, it is additionally realized that the H-SSY molecule retains a flat conformation in the nanocolumns and the in-plane direction of the disk is perpendicular to the long axis of the nanofiber.

In summary, the anisotropically oriented PVP–H-SSY nanofiber mats were successfully fabricated by electrospinning and orientation techniques. Based on the combined results of POM, DSC, 2D WAXD and polarized FTIR, it was realized that H-SSY molecules retaining a flat conformation self-assembled to nanocolumns and formed a glassy columnar N LC phase in the PVP–H-SSY nanofiber. When the PVP–H-SSY nanofiber mat was annealed above the $T_g =$ 180 °C of PVP, the H-SSY nanocolumns further self-organized to crystals. The anisotropically oriented nanofiber mats embedding assembled nanocolumns may open new doors for the practical applications of the electrospun nanofibers in optical, electronic and electro-optic devices.



## Acknowledgements

This research was mainly supported by the Basic Science Research Program (2011-0004900) and the Converging Research Center Program (2011K000776) of the Korean government.

## Notes and references

1 (*a*) V. R. Hoeowitz, L. A. Janowitz, A. L. Modic, P. A. Heiney and P. J. Collings, *Phys. Rev. E: Stat., Nonlinear, Soft Matter Phys.*, 2005, **72**, 041710; (*b*) K.-U. Jeong, A. J. Jing, B. Monsdorf, M. J. Graham, F. W. Harris and S. Z. D. Cheng, *J. Phys. Chem. B*, 2007, **111**, 767; (*c*) J. H. Jung, S.-E. Kim, E. K. Song, K. S. Ha, N. Kim, Y. Cao, C.-C. Tsai, S. Z. D. Cheng, S. H. Lee and K.-U. Jeong, *Chem. Mater.*, 2010, **22**, 4798; (*d*) S. Leng, L. H. Chan, J. Jing, J. Hu, R. M. Moustafa, R. M. Van Horn, M. J. Graham, B. Sun, M. Zhu, K.-U. Jeong, B. R. Kaafarani, W. Zhang, F. W. Harris and S. Z. D. Cheng, *Soft Matter*, 2010, **6**, 100; (*e*) L. Wang, H. Cho, S.-H. Lee, C. Lee, K.-U. Jeong and M.-H. Lee, *J. Mater. Chem.*, 2011, **21**, 60.
2 J. Lydon, *Curr. Opin. Colloid Interface Sci.*, 2004, **8**, 480.
3 H. von Berlepsch, C. Böttcher and L. J. Dähne, *J. Phys. Chem. B*, 2000, **104**, 8792.
4 L. Joshi, S.-W. Kang, D. M. Agra-Kooijman and S. P. J. Kumar, *Phys. Rev. E: Stat., Nonlinear, Soft Matter Phys.*, 2009, **80**, 041703.
5 H.-S. Park, S.-W. Kang, L. Tortora, Y. Nastishin, D. Finotello, S. Kumar and O. D. Lavrentovich, *J. Phys. Chem. B*, 2008, **112**, 16307.
6 (*a*) C. Ruslim, D. Matsunaga, M. Hashimoto, T. Tamaki and K. Ichimura, *Langmuir*, 2003, **19**, 3686; (*b*) K.-U. Jeong, S. Jin, J. J. Ge, B. S. Knapp, M. J. Graham, J. Ruan, M. Guo, H. Xiong, F. W. Harris and S. Z. D. Cheng, *Chem. Mater.*, 2005, **17**, 2852; (*c*) K.-U. Jeong, B. S. Knapp, J. J. Ge, S. Jin, M. J. Graham, F. W. Harris and S. Z. D. Cheng, *Chem. Mater.*, 2006, **18**, 680; (*d*) K.-U. Jeong, D.-K. Yang, M. J. Graham, Y. Tu, S.-W. Kuo, B. S. Knapp, F. W. Harris and S. Z. D. Cheng, *Adv. Mater.*, 2006, **18**, 3229; (*e*) L. Wang, S.-J. Pak, S.-H. Lee, Y.-J. Kim, Y.-B. Kook, S.-W. Kuo, R. M. Van Horn, S. Z. D. Cheng, M.-H. Lee and K.-U. Jeong, *Chem. Mater.*, 2009, **21**, 3838.
7 Q. Zhnag, C. G. Bazuin and C. Barrett, *Chem. Mater.*, 2008, **20**, 29.
8 S. Laschat, A. Baro, N. Steinke, F. Giesselmann, C. Hägele, G. Scalia, R. Judele, E. Kapatstina, S. Sauer, A. Schreivogel and M. Tosoni, *Angew. Chem., Int. Ed.*, 2007, **46**, 4832.
9 D. Adam, P. Schuhmacher, J. Simmerer, L. Haussling, K. Siemensmeyer, K. H. Etzbach, H. Ringsdorf and D. Haarer, *Nature*, 1994, **371**, 141.
10 V. Lemaur, D. A. da Silva Filho, V. Coropceanu, M. Lehmann, Y. Geerts, J. Piris, M. G. Debije, A. M. van de Craats, K. Senthilkumar, L. D. A. Siebbeles, J. M. Warman, J.-L. Bredas and J. Cornil, *J. Am. Chem. Soc.*, 2004, **126**, 3271.
11 A. Greiner and J. H. Wendorff, *Angew. Chem., Int. Ed.*, 2007, **46**, 5670.
12 S. Z. D. Cheng, *Phase Transition in Polymer: The Role of Metastable States*, 2008.
13 R. Hosemann, *X-Ray Diffraction by Polymers*, 1971.

 